EIGHTEENTH EUROPEAN ROTORCRAFT FORUM

BU - 19

Paper N° 137

AN INVESTIGATION OF DYNAMIC STALL THROUGH THE APPLICATION OF LEADING EDGE ROUGHNESS

R.B. Green
Research Fellow

and

R.A.McD. Galbraith
Head of Department

Department of Aerospace Engineering,
University of Glasgow

September 15-18, 1992
AVIGNON, FRANCE

ASSOCIATION AERONAUTIQUE ET ASTRONAUTIQUE DE FRANCE

AN INVESTIGATION OF DYNAMIC STALL THROUGH THE APPLICATION OF LEADING EDGE ROUGHNESS

by

R.B. Green and R.A.McD. Galbraith,
Dept. Aerospace Engineering,
University of Glasgow,
Glasgow,
Scotland.
G12 8QQ

Abstract

The dynamic stall characteristics of a series of aerofoil models performing ramp-up motions are considered. Pressure data show the development and convection of structures at the leading and trailing edges, which indicate differing degrees of what are described as leading edge and trailing edge stall mechanisms. When a transition strip is placed at the leading edge, the characteristics of leading edge stall predominate, and the growth of the structure at the trailing edge is suppressed. In addition the stall vortex convection speed is observed to alter significantly, which is interpreted as a change in the vortex origin, size, strength and trajectory.

Nomenclature

AR	model aspect ratio
c	model chord length (m)
C_m	moment coefficient
C_n	normal force coefficient
C_p	pressure coefficient
R	Re /10^6
r	reduced pitch rate ($\omega c/2U$)
Re	Reynolds number
U	free stream velocity (ms^{-1})
u	stall vortex convection speed (ms^{-1})
x	chordwise position from leading edge (m)
α	incidence (deg)
ω	pitch rate (rad s^{-1})

1. INTRODUCTION

Low speed dynamic stall is characterised by the formation and convection of a powerful, well organised vortex structure (the stall vortex) over a pitching aerofoil's suction surface. If the oscillation frequency and ampitude are high enough the phenomenon may occur on the retreating blade of a helicopter rotor. Thus, since the associated pitching moment and lift coefficients may induce excessive vibration and fatigue loading, limitations are imposed on the vehicle's flight envelope, and an

understanding of the phenomenon, both from a practical and a more fundamental point of view, is needed.

Although the phenomenon has been studied extensively, basic questions concerning the vortex growth mechanism remain. McCroskey at al.[1] investigated the role of the leading edge separation bubble on a NACA 0012 by placing a transition strip at the leading edge. They concluded that bubble bursting was not the basic phenomenon, and suggested that abrupt turbulent separation downstream of the separation bubble was involved in the mechanism that fed the stall vortex. A further investigation by McCroskey et al.[2] attempted to further classify stall types, and the effects of trailing edge separation were studied. It was observed that different aerofoils showed widely varying characteristics, and leading edge, trailing edge, abrupt trailing edge and mixed stall types were observed, although all the aerofoil models tested tended to show more of the leading edge stall characteristics as the dynamic stall intensified.

The dynamic stall of the NACA 0012 aerofoil model has been studied widely, and many descriptions of vortex growth and leading edge type stall are available. Particle Image Displacement Velocimetry data are described by Shih et al.[3], in which particular unsteady flow separation mechanisms were identified. It was observed that the stall vortex grew at the leading edge, and induced a counter-rotating vortex beneath it. This structure then lifted the stall vortex away from the surface. Particular sites at the leading edge have also been observed to be sources of vorticity for the stall vortex (Acharya & Metwally[4]); the vorticity feeding the stall vortex was seen to originate primarily from an area 1% of chord either side of the aerofoil nose.

Studies of the NACA 0015 aerofoil by Visbal & Shang[5], however, have suggested the additional existence of a 'shear layer vortex' developing over the trailing edge region of the aerofoil. This structure will interact with the development and convection of the stall vortex; although exactly how is not clear. What is important is that an aerofoil model prone to trailing edge separation shows different characteristics to a leading edge stall type model.

The present work describes test results from a series of aerofoil models which predominantly display trailing edge stall characteristics. Particular emphasis is placed on the effects of a transition strip placed at the leading edge. It is a continuation of the work reported by Green et al.[6, 7], in which anomolous results of the stall vortex convection speed were described. Surface pressure and stall vortex convection speed data are used to quantify the differences between tests with and without the leading edge sand strip.

2. THE UNIVERSITY OF GLASGOW UNSTEADY AERODYNAMICS TESTING FACILITY

The general arrangement of the model in the wind tunnel is illustrated in figure 1. Four models are discussed in this report, namely the NACA 0015, the 21% thick M13 model which is designed for use in vertical axis wind turbines, the GUVA10, which is essentially a NACA 0018 with a leading edge resembling a NACA 0012, and a NACA 0012 model. The four aerofoil profiles are shown in figure 2. The M13, GUVA10 and NACA 0012 models had chord lengths of 0.55m, while the NACA 0015 had a chord length of 0.275m. All of the models were constructed of a fibre glass skin filled with an epoxy resin. Each model had a span of 1.61m, and the NACA 0015 model spar was made of steel, while the other model spars were made of aluminium. The models were mounted vertically in the University of Glasgow's Handley-Page wind tunnel, which is

a closed return type with a 1.61mx2.13m working section. Thus the NACA 0015 had an aspect ratio and blockage coefficient of 5.84 and 0.13, while the other three models' figures were 2.92 and 0.26. The effects of these different geometries are discussed later.

A linear hydraulic actuator and crank mechanism was used to pivot the aerofoil model about its quarter chord. Instantaneous aerofoil incidence was measured using a linear angular potentiometer geared to the model's tubular support. The dynamic pressure in the working section was obtained from the difference between the static pressure in the working section, about 1.2m upstream of the leading edge of the large chord models, and the static pressure in the settling chamber. Thirty ultra-miniature pressure transducers (type KULITE XCS-093-PSI G) were installed below the centre span of each model, and their locations are shown in figure 2. After signal conditioning the outputs of the pressure transducers were passed to a sample and hold module. For the M13, GUVA10 and NACA 0012 models data logging was performed using a DEC MINC. Five data sweeps containing 256 samples from each of the pressure transducers were recorded at up to 550Hz using this system. Data from the NACA 0015 were logged using a Thorn-EMI BE256 programmed by an IBM model 80. Six data sweeps containing 1024 samples per channel at up to 50KHz were recorded. After sampling the data were reduced, averaged and stored on a DEC MicroVAX for subsequent analysis.

3. RESULTS

All the aerofoil models were tested for a variety of motion types, although only data from ramp-up tests will be presented here. In such a test the aerofoil model is pitched at a uniform rate from α=-1° to 40°. Small non-linearities are, of course, encountered at both the start and finish of the motion. The nominal Reynolds numbers for the large chord and NACA 0015 models are 1.5 million and 0.8 million respectively, and the Mach number for all the tests is 0.12.

The collected pressure data are presented in a pseudo-three-dimensional form (e.g. figure 3a), where the development of the chordwise pressure distribution is shown as a function of incidence. This renders the pressure manifestations of any flow structures visible. Quarter chord pitching moment coefficient is plotted alongside the pressure data.

Two test cases are presented for the M13, GUVA10 and NACA 0015 models, namely free transition (clean leading edge) and fixed transition (sand strip leading edge). Only free transition data are available for the NACA 0012. The prime reason for the forced transition was to attempt to make the flow over the NACA 0015 model more comparable with its larger chord counterparts. The transition strip used sand in a similar manner to that described by Landon[8], and consisted of sand grains of average diameter 0.15mm distributed around the leading edge to 2% chord on both surfaces. So profound were its effects upon the dynamic stall performance that it is now incorporated in all the tests at the University of Glasgow. As will be observed in section 3.2, however, a more comprehensive treatment of which 'trip' to use is required.

3.1 Clean leading edge results

Shown in figures 3a, b, c and d are the clean leading edge results for the the aerofoils considered.

Clean leading edge M13 at r=0.032

On figure 3a it may be observed that as incidence increases the leading edge suction likewise increases. In addition at α=25°, the pressure is nearly constant from x/c=0.25 to the trailing edge, which could be interpreted as the result of gradual encroachment of trailing edge separation. Above this incidence a region of increased suction (indicated on the figure) can be seen to develop near to the trailing edge, and there is a corresponding sharp decrease in C_m. The suction bulge enlarges (in both extent and maximum suction) as α increases, and it also appears that its centre moves towards the mid-chord. These changes are reflected by rises in the magnitudes of C_m and C_n. Leading edge suction collapse at α=30° is followed by a wave travelling down the chord. Development of the suction bulge ceases when it meets the wave from the L.E. around the mid-chord location. Maximum bulge suction coincides with $C_{n\,max}$, and further decreases in C_m accompany the motion of the suction bulge towards and over the trailing edge.

Clean leading edge GUVA10 at r=0.032

A similar pattern of events to that of the M13 test emerges for the GUVA10 data (figure 3b) although important differences may be seen. A bulge in the pressure distributions develops from α=27°, with its initial development occurring closer to the mid-chord. The bulge ceases development when the leading edge suction collapses (here occurring at a slightly lower incidence for the M13) and is followed by the convection down the chord of a strong pressure disturbance from the leading edge. The speed of this wave can be found by measuring the timing of the associated localised suction peaks (see section 3.3). Between 5% and 59% chord the speed of the wave is 63% of the free stream speed. Downstream of x/c=0.59 the speed is approximately halved, which is presumably the result of the interaction with the suction bulge structure; the nature of this interaction is unclear.

Clean leading edge NACA 0015 at r=0.03

Figure 3c shows the pressure data for the NACA 0015. The suction bulge first appears close to the mid-chord, and is apparently stronger than for the GUVA10 case. The pressure wave travelling down the chord after suction peak collapse can again be seen, and again development of the suction bulge ceases when the L.E. wave meets it. In this case the convection speed of the wave is uniform from x/c=0.10 to 0.83 at u/U=0.42.

Clean leading edge NACA 0012 at r=0.032

The pressure data for this test, shown in figure 3d, are quite different from the data for the other three aerofoils. Most obvious is the evident lack of the trailing edge suction bulge development. The stall vortex first appears in the pressure data at about 10% chord, and convection starts just after leading edge suction collapses. The speed of the vortex pressure wave is uniform along the entire length of the chord at u/U=0.29.

Summary of clean leading edge data

The salient features of the pressure data described above are the development of the suction bulge, and the stall vortex induced pressure wave travelling from the leading edge. Each of the aerofoils tested shows these features to differing degrees. Even allowing for Reynolds number effects on the NACA 0015 data, it appears that the origin of the suction bulge moves forward with decreasing aerofoil thickness, while the leading edge wave disturbance becomes stronger as the leading edge is sharpened (the GUVA10 and the NACA 0012 have the sharpest leading edges). Thus the NACA 0012 data combine the above two effects, so virtually no trailing edge suction bulge development and a very strong L.E. disturbance are observed.

3.2 Results for tests with the leading edge transition strip

Static data

Figure 4 shows a comparison of static test data for the NACA 0015 at R=1.0 (nominal). The clean leading edge data indicates stall at α=17°, and the hysteresis loop is about 3° wide at the most. The gentle nature of the stall reflects trailing edge separation and maximum C_n is 1.2. Stall for the sand strip test, however, occurs much earlier at about 9° incidence with a $C_{n\,max}$ of 0.8. The lift curve slope falls below that of the clean leading edge case at α=5°, and there is no hysteresis loop.

The relative features of the sand strip case indicate significant boundary layer thickening. In this respect the leading edge sand strip has disturbed the boundary layer more than necessary, so a higher Reynolds number test is probably *not* being reasonably simulated. Examination of the pressure data shows that the stall is still of a trailing edge type. Both the M13 and GUVA10 models show similar changes when the sand strip is applied.

M13 with leading edge sand strip at r=0.036

In figure 5a it can be seen that the dynamic stall of the M13 with the leading edge trip is quite different from the clean leading edge test shown in figure 3a. Leading edge suction collapses at a lower incidence (24° compared to 30°). A very strong pressure wave then travels down the chord at an assessed constant speed of u/U=0.27. At α=22° a region of localised suction starts to develop close to the trailing edge, which reaches a maximum at α=27°, when the disturbance from the leading edge is at x/c=0.25 (the maximum extent of the trailing edge suction bulge is over the last 30% of chord). The initial development of the suction bulge is similar to the clean leading edge case, except that there is a phase lead of some 3°. Note that as the bulge develops, the magnitude of C_m increases, and then falls as the structure convects off the trailing edge. There is then a second, much stronger C_m peak as the stall vortex from the leading edge passes over the trailing edge.

GUVA10 with leading edge sand strip at r=0.036

The flow development for the GUVA10 with the sand strip, shown in figure 5b, is very similar to the case described above. Leading edge suction collapse occurs earlier at α=19°. As with the M13 test a region of localised suction briefly grows near to the trailing edge, although in this case it is much weaker and less extensive. The phasing of the growth of the suction bulge is the same, with maximum suction at x/c=0.83

occurring when the wave from the leading edge is at x/c=0.16. A small minimum in the C_m-α response before the true minimum value of C_m is also observed. The leading edge pressure wave convects uniformly along the chord at u/U=0.23, which is a slightly lower speed than for the M13 case.

NACA 0015 with leading edge sand strip at r=0.027

Features observed in the pressure data for the M13 and GUVA10 tests are seen again in the data for the NACA 0015 test. Leading edge suction collapse occurs at α=19°, followed by convection down the chord of a strong disturbance at a uniform speed of u/U=0.20. Growth of the trailing edge suction bulge is very limited, and the associated local C_m minimum is small. In addition phasing of the events is similar to the other aerofoil tests, with maximum trailing edge suction at x/c=0.83 occurring when the leading edge wave is at x/c=0.18.

Summary of leading edge sand strip pressure data

The pressure data for the sand strip tests differ greatly from the clean leading edge cases. A strong dynamic stall vortex is shed directly from the leading edge. A structure in the trailing edge region forms, although further development is suppressed as the stall vortex convects. Stall occurs relatively early for all the tests.

3.3 Stall vortex convection speed

The stall vortex convection speed can only be measured accurately if the passage of the vortex causes a well defined pressure wave. Lorber & Carta[9] determined the convection speed by measuring the timing of the associated suction peaks, and this method has been adopted by Green et al.[6] and in the present paper.

No data are available from the clean L.E. M13 tests across the entire pitch rate range since the suction peaks are too poorly defined. The same problem was encountered with the clean L.E. GUVA10 data, except at the very highest pitch rates, where the speed of the leading edge wave is u/U=0.63 in the range 0.05<x/c<0.59. Downstream of this the convection of the trailing edge suction bulge disturbance affects the data.

Data are available for the NACA 0015 in the range 0.01<r<0.03, although below r=0.02 the results are very inaccurate and only the overall trend should be considered. These data are shown in figure 6, where convection speed is plotted as a function of reduced pitch rate. It appears that as pitch rate increases from 0.01 the convection speed falls rapidly and then takes on a constant value of about 0.4 above r=0.02. Also shown are convection speed data for a NACA 0015 model of the same physical size as the M13, GUVA10 and NACA 0012 models; this model has half the aspect ratio and twice the blockage of the NACA 0015 model data described in this paper. When the overall level of scatter is considered, the data from the two NACA 0015 models are effectively the same.

The wave disturbance for the NACA 0012 is very strong across the entire pitch rate range, and as a consequence measurements of convection speed were obtained down to r=0.006. Above r=0.01 the convection speed is independent of reduced pitch rate with a mean value of u/U=0.28, and there is a small amount of scatter in the results. Below r=0.01, the speed appears to rise slightly, although this may be an accuracy effect.

Also shown on figure 6 are the data for the tests with the leading edge sand strip, where vortex convection is very well defined over a wide range of r. For all the aerofoil models the convection speed is independent of pitch rate down to r=0.01, while below this the convection speed appears to increase with decreasing r. This may be an effect

of decreasing accuracy as the stall vortex becomes less well defined, although it must be noted that all the models show the same trend. The average convection speeds for the M13, GUVA10 and NACA 0015 models are 0.26, 0.24 and 0.19 respectively.

4. DISCUSSION

Pressure and stall vortex convection speed data have been presented for five different aerofoil models. In addition the results from two NACA 0015 models of different aspect ratio and blockage were described. These results supported the thesis that wind tunnel contraints did not seriously affect the gross features of the dynamic stall as observed in the present tests. The NACA 0015 data described may therefore be compared objectively with the data from the other aerofoil models (a more comprehensive discussion of Re and constraint effects is given by Green & Galbraith[10]).

The data presented highlight distinct differences between dynamic stalling predominantly towards the trailing edge and that occurring close to the leading edge. The M13 aerofoil in the clean configuration (figure 3a) appears to exhibit trailing edge separation (characterised by constancy of the Cp profile), which, as it penetrates towards the leading edge, shows signs of re-attachment near to the trailing edge. This is characterised by the strong pressure recovery there. The pressure profile then develops an obvious bulge followed by leading edge suction collapse. The GUVA10 and the NACA 0015 sections (figures 3b and 3c) have similar but weaker developments, and, in addition, show a much stronger L.E. shed vortex after the suction collapse. Further growth of the suction bulge ceases when the wave following leading edge suction collapse meets it, and the structures then convect off the aerofoil surface. The GUVA10 data in particular suggest that the L.E. and T.E. structures interact as they are still developing; initial growth of the T.E. structure is similar to the M13 case, although it soon becomes overwhelmed by the more dominant L.E. vortex. In contrast to this, the NACA 0012 section pressure history (figure 3d) does not exhibit any significant signs of the bulge just described, but is clearly dominated by a strong L.E. vortex. This is a predominantly L.E. type of stall.

From a solution of the Navier-Stokes equations of the dynamic stall of a NACA 0015 section, Visbal & Shang [5] described the existence of a 'shear layer vortex', which was observed to develop over the aft portion of the aerofoil surface. As the leading edge stall vortex convected along the aerofoil chord they observed that the shear layer vortex distorted considerably, and was squeezed under the L.E. vortex. Shih et al.[3] described both Particle Image Displacement Velocimetry data and solutions of a Navier-Stokes code for a NACA 0012. Here there was also evidence of the 'shear layer vortex', although it did not appear to develop to as great an extent as the NACA 0015 case of Visbal & Shang[5], and the development of the leading edge vortex was the predominant feature. Although the Reynolds number of the above simulations is considerably lower than that of the present tests, the presence of a shear layer vortex could explain the development of the trailing edge suction bulge. Obviously the cause of the suction bulge warrants further investigation.

In 'static' tests the models with the leading edge sand strips stalled from the trailing edge, while during ramp-up tests a very strong stall vortex was seen to spring from the leading edge in a fashion similar to the NACA 0012 data. The most interesting case is that of the M13 where there is substantial development of the trailing edge suction

bulge, i.e. the characteristics of trailing edge type dynamic stall as described above are also developing. Both the NACA 0015 and GUVA10 models show this feature, although not to as great an extent. Initial growth of the suction bulge occurs earlier than in the clean leading edge case, since trailing edge separation starts at a lower incidence, which is presumably the result of increased boundary layer thickness caused by the sand strip. Further growth of the nascent trailing edge structure is suppressed by convection of the leading edge vortex; maximum suction at x/c=0.83 occurs when the L.E. vortex is at x/c=0.16. If the T.E. structure is vortical in nature, then the growth and convection of the much enhanced leading edge vortex will deplete the supply of vorticity to it.

Even though the clean L.E. M13, GUVA10 and NACA 0015 models have been classified as stalling dynamically, principally via a trailing edge mechanism, the role of the leading edge is still of great importance, since the convection of the wave from the leading edge appears to stop further development of the T.E. structure. One of the main differences between the clean and sand strip L.E. tests is the extent to which the T.E. structure grows, although in both cases it appears that its ultimate fate is controlled by the L.E. vortex.

While no attempt will be made to propose a mechanism for the growth of stall vortices at the leading edge, it must be accepted that the application of the leading edge sand strip causing the above observations introduces a substantial disturbance to the boundary layer. These disturbances are amplified to produce a very powerful leading edge vortex compared to the clean leading edge case. Whether or not this mechanism is the same as that which causes the stall vortex to develop at or near to the leading edge in the case of an aerofoil with a sharp leading edge (e.g. the NACA 0012 or the SSC-A09 used by Lorber & Carta[9]) is outwith the scope of the present paper. The boundary layer over a sharp nosed aerofoil experiences a severe adverse pressure gradient before it breaks down, while that encountered by the boundary layer over the present models with a sand strip is insignificant by comparison. However, the latter case starts with a much greater level of disturbance. In the present context, the clean L.E. GUVA10 tests may be seen as an extension to the clean L.E. NACA 0018 tests. The NACA 0018 test (not shown in this report) shows growth of the suction bulge in the mid-chord region, but only a very weak wave from the leading edge is seen. The sharper L.E. of the GUVA10 strengthens the L.E. wave and diminishes the T.E. suction bulge, and the sand strip GUVA10 virtually eliminates the T.E. disturbance.

Significant differences between the clean and sand strip L.E. stall vortex convection speed results were observed. For the M13 model, no clean L.E. measurements are available because the vortex path is too poorly defined on the pressure trace. Data for the GUVA10 were only obtained at the very highest pitch rate. Therefore the discussion of the differences in convection speed is confined to the NACA 0015 tests, where data across the entire pitch rate range are available. At r=0.022, where the clean L.E. case has a very well defined vortex path, the values of the convection speed are u/U=0.4 and 0.2 for the clean and sand strip cases respectively. The most significant difference between the two data sets is the apparent origin of the stall vortex; for the clean L.E. case the vortex appears to originate just upstream of the mid-chord, while for the sand strip case it springs from the leading edge area. The different speeds and origins suggest different vortex trajectories; the aerofoil surface may be modelled by a mirror effect, in which case a slow convection speed suggests that the vortex is travelling close to the aerofoil surface, while faster speeds may occur when it is further away. Support for this postulation can be inferred from the pressure data, since the vortex induced

suction peaks are sharp for the sand strip (slow) case, and are more poorly defined for the clean (fast) case. Additional data, probably in the form of flow visualisation, is needed for further discussion of this hypothesis.
The stall vortex will interact with other flow structures as it convects. Varying degrees of interaction may also account for the changes in the stall vortex convection speed, which is an important result if the trailing edge suction bulge indicates the presence of a shear layer vortex. Green et al.[6] reported anomalous results of the stall vortex convection speed; Lorber & Carta[9] found that u/U showed a linear dependence on r, while data from tests at the University of Glasgow suggested no functional dependence. Lorber & Carta's data were from a 9% thick aerofoil model which showed no development of trailing edge structures, while the University of Glasgow data were from thicker aerofoils with more rounded leading edges. Again, flow visualisation data is needed.
The present work has illustrated that the detailed development of an aerofoil's dynamic stall characteristics can be significantly altered by a change in the leading edge flow conditions. Disturbances grow at the leading edge and in the trailing edge region, and the relative amounts of each are dependent upon the aerofoil thickness and the conditions at the leading edge. As well as posing fundamental questions as to the nature of dynamic stall, the present work has ramifications upon the performance of rotor-craft and aircraft that may utilise the dynamic stall phenomenon. For example, after leading edge erosion, a retreating helicopter blade may stall dynamically in the fashion of the sand strip tests, when the design conditions specified otherwise. In addition, the different dynamic stall parameters such as stall incidence and vortex convection speed would be greatly different from those programmed into a flight control system.

5. CONCLUSIONS

The application of leading edge roughness was observed to significantly alter the salient features of the dynamic stalling process. In particular the development of the trailing edge structure was virtually eliminated, while the leading edge stall vortex appeared to be strengthened.
Stall vortex convection speed data for the clean and sand strip leading edge cases were significantly different from each other. For the clean L.E. NACA 0015, the convection speed showed a pitch rate dependency at low pitch rate, and took a constant value at higher pitch rate. For the sand strip tests, the convection speed was constant across the entire pitch rate range, with the mean value for the NACA 0015 tests being half the high pitch rate mean value for the clean leading edge case.

ACKNOWLEDGEMENTS

The work was carried out with the financial assistance of the Science and Engineering Research Council, with significant contributions from the ETSU and VAWT Ltd, the United States Air Force Office of Scientific Research, the DRA and Westland Helicopters. In addition the assistance of the technical staff in the Department of Aerospace Engineering, University of Glasgow, is greatly appreciated.

REFERENCES

1. McCroskey, W.J., Carr, L.W. & McAlister, K.W. 'Dynamic stall experiments on osillating airfoils' A.I.A.A. Journal, Vol. 14, p57, (1976)

2. McCroskey, W.J., McAlister, K.W., Carr, L.W., Pucci, S.L., Lambert, O. & Indergrand, R.F. 'Dynamic stall on advanced airfoils' Journal of the American Helicopter Soc., Vol. 26, p40, (1981)

3. Shih, C., Lourenco, L., Van Dommelen, L. & Krothapalli, A. 'Unsteady flow past an airfoil pitching at a constant rate' A.I.A.A. Journal, Vol. 30, p1153, (1992)

4. Acharya, M. & Metwally, M.H. 'Unsteady pressure field and vorticity production over a pitching airfoil' A.I.A.A. Journal, Vol. 30, p403, (1992)

5. Visbal, M.R. & Shang, J.S. 'Investigation of the flow structure around a rapidly pitching aerofoil' A.I.A.A. Journal, Vol. 27, p1044, (1989)

6. Green, R.B., Galbraith, R.A.McD. & Niven, A.J. 'Measurements of the dynamic stall vortex convection speed' Paper N° 91-68, Presented at 17th European Rotorcraft Forum, Berlin, September 1991.

7. Green, R.B., Galbraith, R.A.McD. & Niven, A.J. 'The convection speed of the dynamic stall vortex' University of Glasgow, Aero. Rept. 9202, United States Air Force Office of Scientific Research Contract AFOSR-89-0397, January 1992.

8. Landon, R.H. 'A description of the A.R.A. two-dimensional pitch and heave rig and some results from the NACA 0012 wing' A.R.A. Memo N° 199, (1977)

9. Lorber, P.F. & Carta, F.O. 'Unsteady stall penetration experiments at high Reynolds number' AFOSR TR-87-1202, UTRC Rept. N° R87-956939-3, (1987)

10. Green, R.B. & Galbraith, R.A.McD. 'The effect of wind tunnel constraint on unsteady aerodynamics experiments' Paper N° 92-3.6.4, to be presented at 18th ICAS conference, Beijing, China, September 1992.

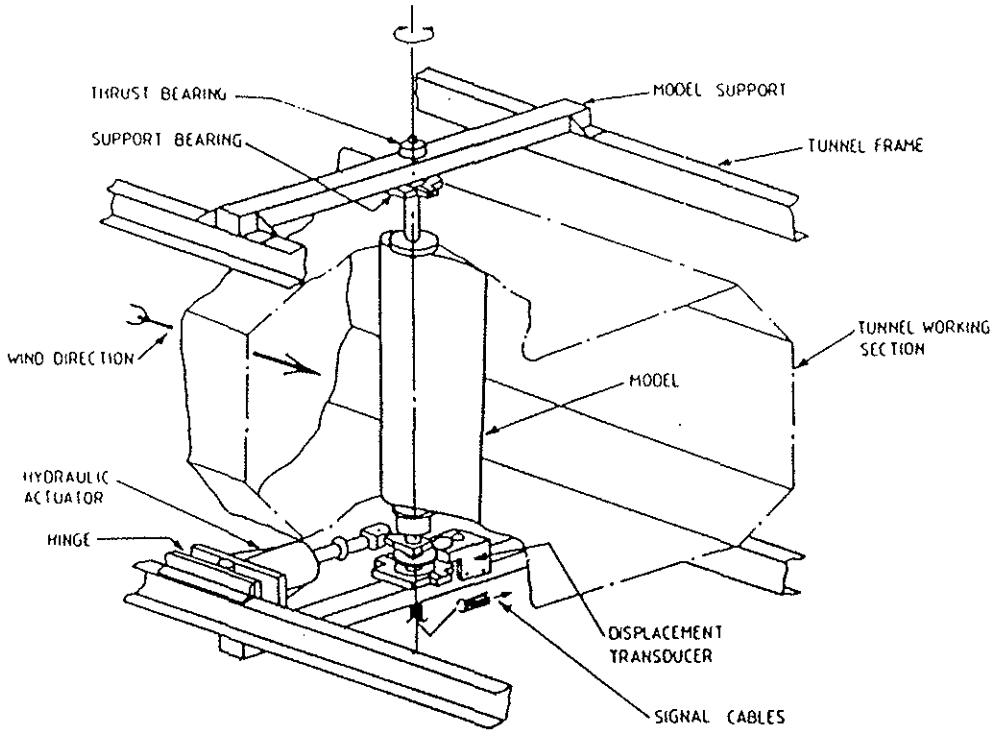

Figure 1 The University of Glasgow Handley-Page wind tunnel and unsteady aerodynamics facility

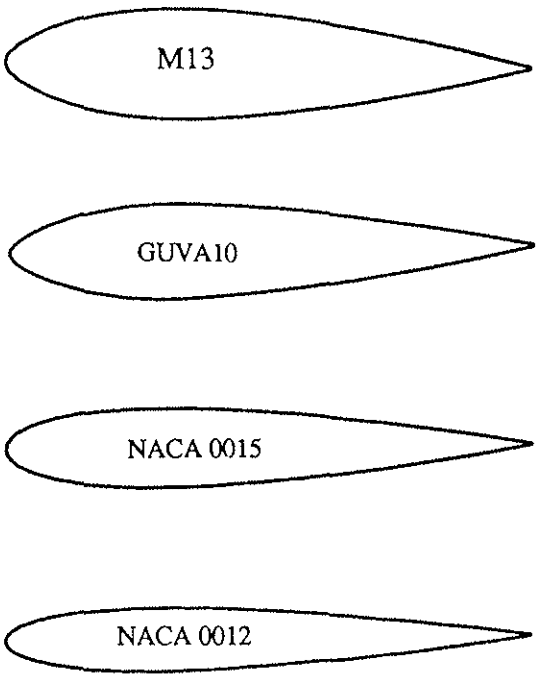

TRANSDUCER Nº.		
SURFACE		
UPPER	LOWER	X/C
1	30	0.98
2	29	0.95
3	28	0.83
4	27	0.70
5	26	0.59
6	25	0.50
7	24	0.37
8	23	0.26
9	22	0.17
10	21	0.10
11	20	0.05
12	19	0.025
13	18	0.01
14	17	0.0025
15	16	0.0003

Figure 2 Aerofoil profiles and pressure transducer locations.

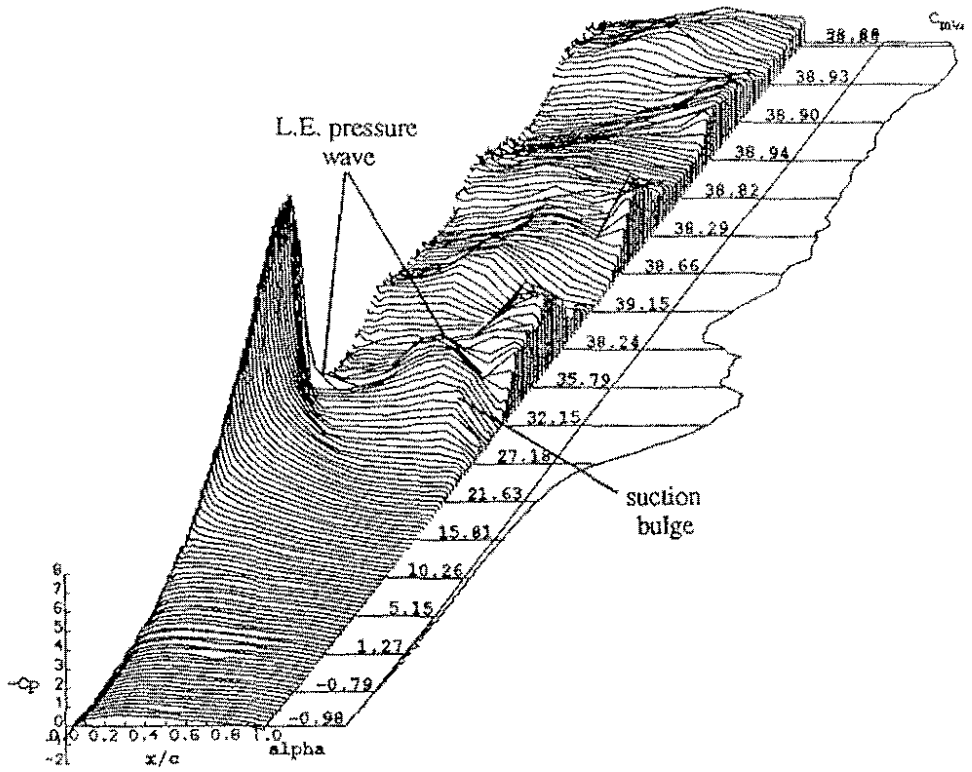

Figure 3a Pressure data for the clean leading edge AHAVAW ramp-up test at r=0.032 and R=1.5. The salient features are indicated.

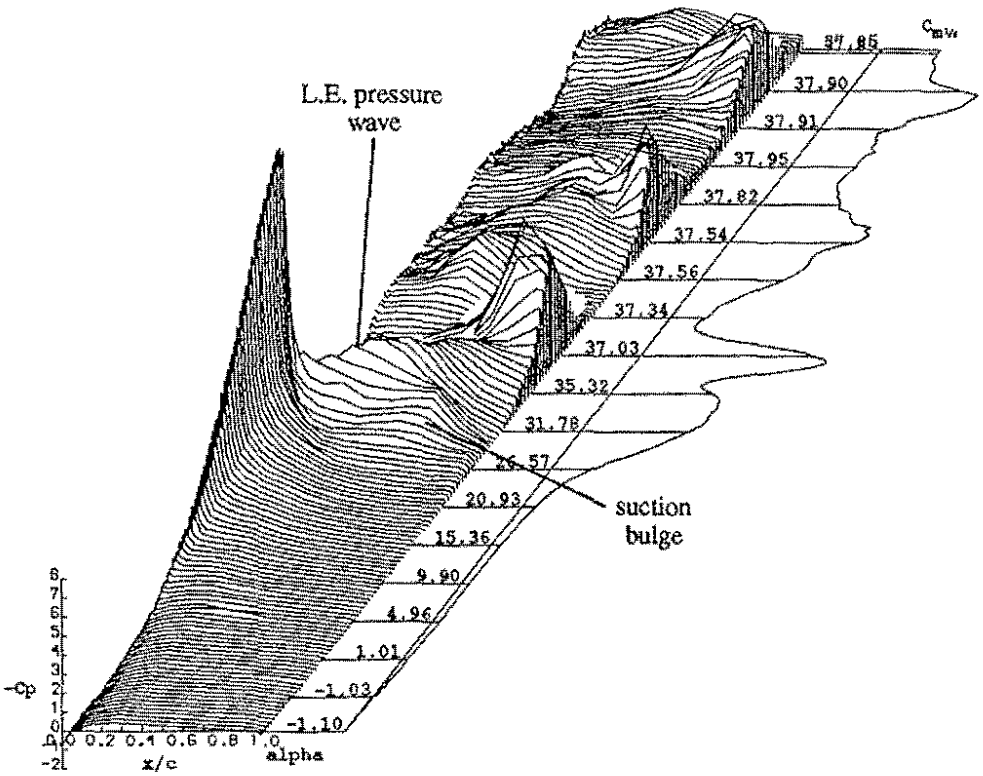

Figure 3b Pressure data for the clean leading edge GUVA10 ramp-up test at r=0.032 and R=1.5. The salient features are indicated.

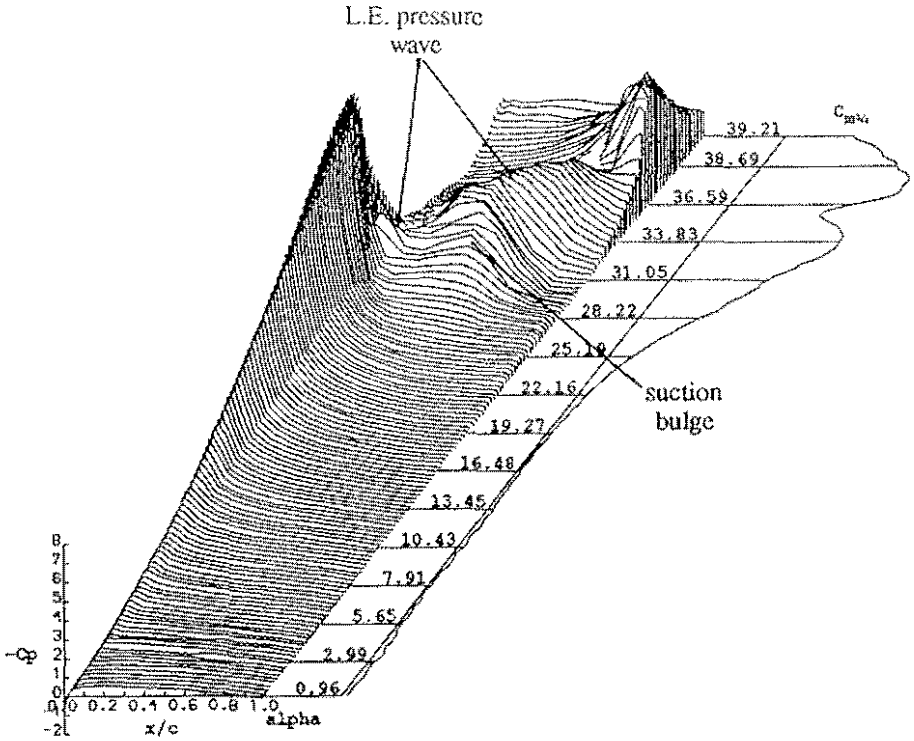

Figure 3c Pressure data for the clean leading edge NACA 0015 ramp-up test at r=0.03 and R=0.8. The salient features are indicated.

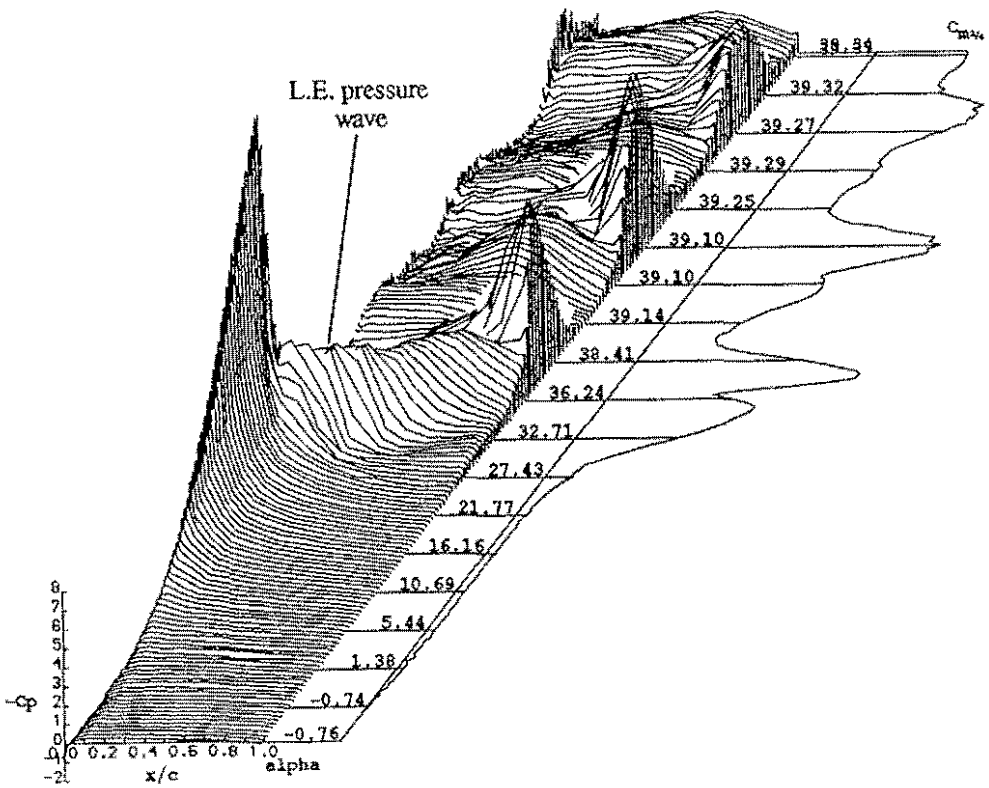

Figure 3d Pressure data for the clean leading edge NACA 0012 ramp-up test at r=0.032 and R=1.5. The salient features are indicated.

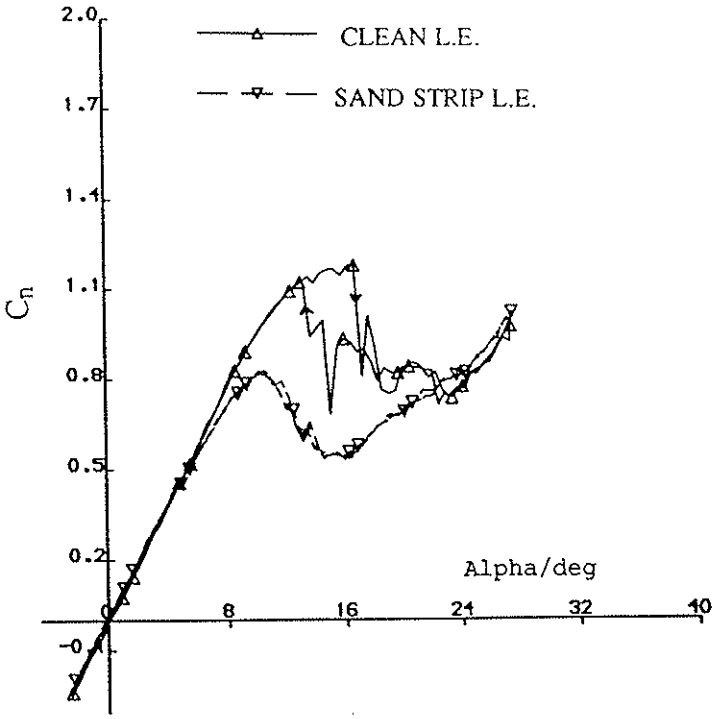

Figure 4 C_n plotted against α for NACA 0015 static data at R=1.0. Clean and sand strip leading edge tests are shown.

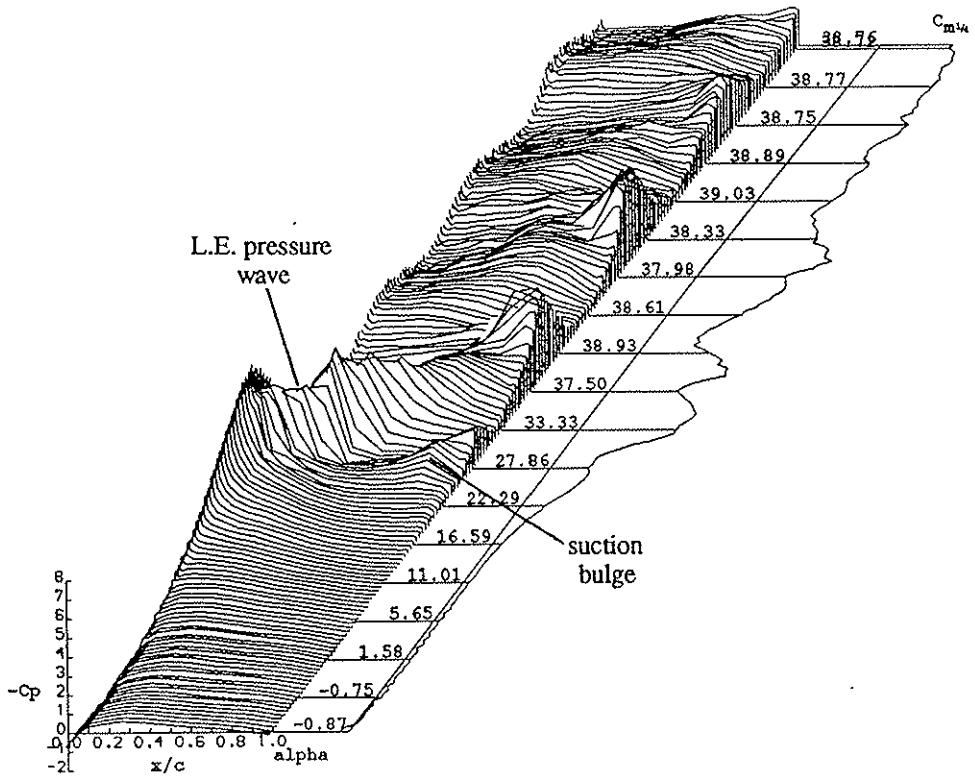

Figure 5a Pressure data for the sand strip AHAVAW ramp-up test at r=0.036 and R=1.5. The salient features are indicated.

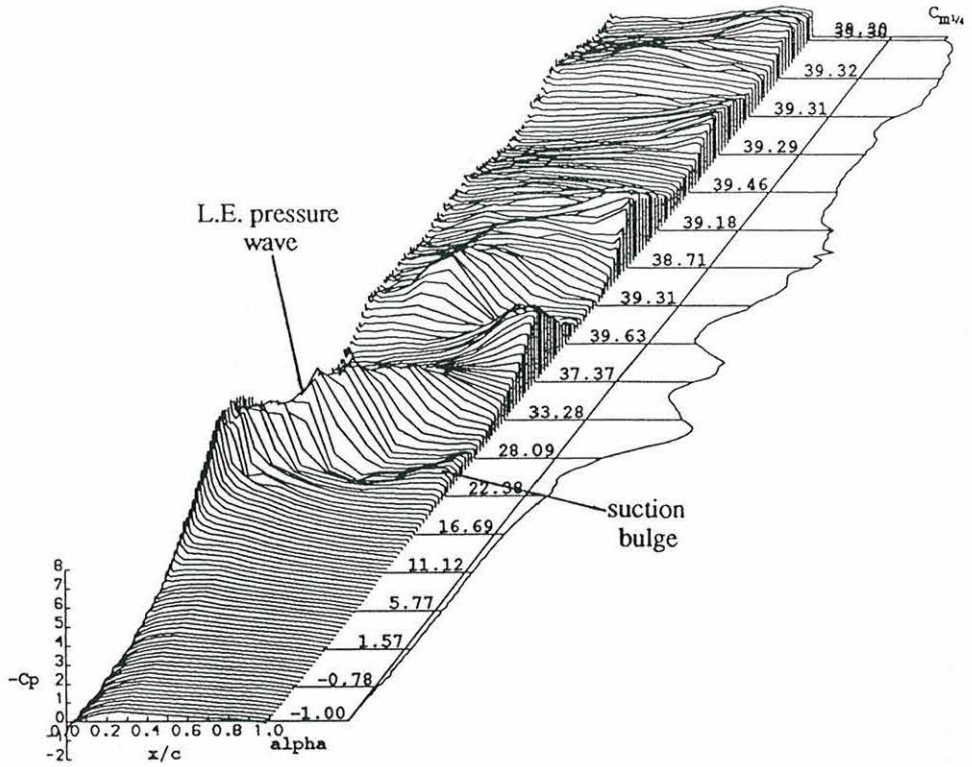

Figure 5b Pressure data for the sand strip GUVA10 ramp-up test at r=0.036 and R=1.5. The salient features are indicated.

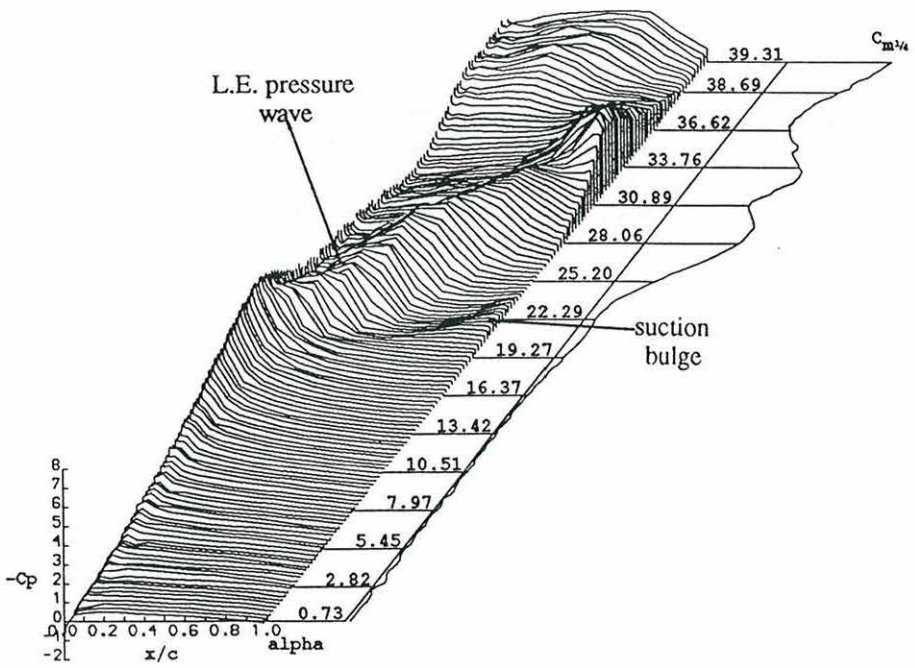

Figure 5c Pressure data for the sand strip NACA 0015 ramp-up test at r=0.027 and R=0.85. The salient features are indicated.

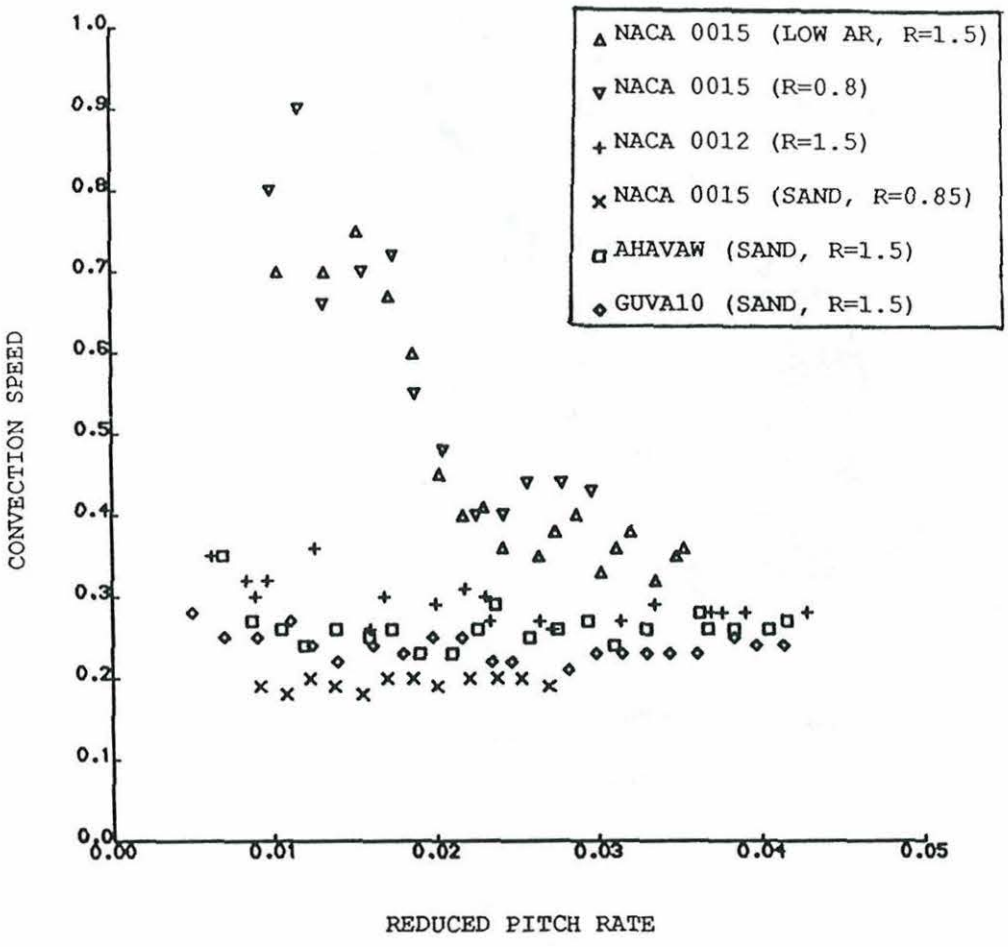

Figure 6 Vortex convection speed plotted as a function of reduced pitch rate. The low AR NACA 0015 data are from the exactly same test conditions (including aspect ratio and blockage) as the AHAVAW and GUVA10 tests.